Effect of global and regional SST biases on the East Asian Summer Monsoon in the MetUM GA7 and GC3 configurations

Climate Dynamics
https://doi.org/10.1007/s00382-023-06954-w

ORIGINAL ARTICLE

Effect of global and regional SST biases on the East Asian Summer Monsoon in the MetUM GA7 and GC3 configurations

Armenia Franco-Díaz[1,2] · Nicholas P. Klingaman[2,4] · Andrew G. Turner[2,3] · Buwen Dong[2] · Liang Guo[2]

Received: 23 December 2022 / Accepted: 7 September 2023

Abstract

Climate-length experiments of the Met Office Unified Model Global Atmosphere 7.0 (GA7) and Global Coupled 3.0 (GC3) configurations are evaluated against observations and reanalyses for the simulation of the East Asian summer monsoon (EASM). The results show systematic model biases, such as overestimated rainfall over southern China and underestimated rainfall over northern China, suggesting a monsoon that does not penetrate northward enough. We evaluate the effects on the EASM of regional errors in sea-surface temperature (SST) conditions in three regions: the Pacific, the Indian, and the Atlantic Oceans. The global SST biases in GC3 configuration substantially shift the EASM seasonal cycle: a late northward progression of the EASM in the early/mid-monsoon season, and an early retreat of the monsoon that also reduces rainfall over most of northern China. The EASM seasonal rainfall bias in the EASM region is linked to changes in the locations and strength of the western North Pacific subtropical high, which is associated with biases in local evaporation and moisture transport towards South China. GC3 biases in the El Niño-Southern Oscillation (ENSO) and the Indian Ocean Dipole (IOD) teleconnection pathways also influence the EASM biases. GC3 biases weaken the ENSO teleconnection to the EASM and cause a strong dry bias in southeast China during developing El Niño.

Keywords MetUM · ENSO · IOD · Interannual variability

1 Introduction

East Asian Summer Monsoon (EASM) rainfall is crucial for one of the most densely populated regions in the world. The population of China strongly depends on EASM rainfall for socio-economic development, such as agriculture, industry, transportation, and infrastructure systems. The EASM is subject to interannual variability that induces floods and droughts and can cause casualties and economic losses (Song and Zhou 2014; Jiang et al. 2021). Therefore, it is necessary to develop weather and climate models that can accurately predict variability and projected change in summer monsoon rainfall over China. Despite recent successes in seasonal predictions for specific regions in China [e.g., the Yangtze River Valley forecast from the Climate Science for Service Partnership China; Li et al. (2016)], the simulation of summer monsoon rainfall in global numerical models is still challenging. Models often overestimate rainfall in southern China and underestimate rainfall in northern China. For example, in the Coupled Model Intercomparison Project Phase 3 (CMIP3) and the Coupled Model Intercomparison Project Phase 5 (CMIP5) atmospheric general

✉ Armenia Franco-Díaz
armenia.franco-diaz@kit.edu

Nicholas P. Klingaman
n.p.klingaman@reading.ac.uk

Andrew G. Turner
a.g.turner@reading.ac.uk

Buwen Dong
b.dong@reading.ac.uk

Liang Guo
l.guo@reading.ac.uk

[1] Institute of Meteorology and Climate Research, Karlsruhe Institute of Technology, 76131 Karlsruhe, Germany

[2] National Centre for Atmospheric Science, Department of Meteorology, University of Reading, Reading RG6 5ES, UK

[3] Department of Meteorology, University of Reading, P.O. Box 243, Reading, RG6 6ET, UK

[4] Citadel Investment Group, Moor House, 120 London Wall, London EC2Y 5ET, UK

Published online: 19 October 2023

circulation models (AGCMs), these rainfall biases are often associated with a weak and southeastward shifted western North Pacific subtropical high (WNPSH), which is linked to a southward shift in moisture transports to East Asia (EA; Song and Zhou 2014; He and Zhou 2014). Also, coupled general circulation models (CGCMs) underestimate the southeast-northwest precipitation gradient, show a deficient strength of the EASM circulation, and overestimate the spatial and magnitude of interannual precipitation variability in EA (Jiang et al. 2016). The Met Office Unified Model (MetUM) produces too much rainfall in southern China and too little rainfall in northern China [e.g., MetUM Global Atmosphere 6.0; Stephan et al. (2018)]. Guo et al. (2020) identified systematic errors of MetUM atmosphere-only and atmosphere-ocean coupled configurations in simulating the moisture sources of East Asian precipitation. Their results suggest that MetUM precipitation biases in EA are linked to underestimated moisture contributions from the tropical Indian Ocean and overestimated contributions from the Eurasian continent.

Other hypothesised sources of EASM systematic model errors include biases in the large-scale meridional tropospheric temperature gradient (Dai et al. 2013) and coarsely resolved topography over EA (Wu et al. 2017). The latter is associated with an underestimated ascent over the mountains of subtropical EA and the Tibetan Plateau. This creates overestimated southerly winds and, compared with observations and high-resolution models, reduces East Asian pre-summer precipitation further north. Another source of hypothesised systematic errors in the thermal forcing is biasing in Pacific and Indian Ocean SSTs. The latter is associated with the representation of the Walker circulation and wave propagation from the Indian to the Pacific Oceans (Wang et al. 2013; Lee et al. 2013). Finally, the monsoon front is often too weak in models and shifted south (Kusonoki et al. 2006), which leads to a wet bias in southern China. These biases are associated with errors in representing the large-scale circulation in the Pacific and the land-sea temperature contrast (Lau and Ploshay 2009; Li et al. 2019).

The representation of the EASM interannual variability and its relationship with interannual modes of variability, such as the El Niño-Southern Oscillation (ENSO; Wang et al. 2008; Liu et al. 2008), has also been studied. Observed El Niño (La Niña) winters correspond to wetter (drier) summers along EA in the following year (Li and Zhou 2012). Wang et al. (2000) suggested that the EASM is influenced by El Niño (La Niña) through anomalous lower-tropospheric circulations over the western North Pacific (WNP). This anomalous anticyclone (cyclone) effect persists over winter and the following summer through positive atmosphere-ocean feedback. Other studies have suggested that this delayed correspondence implies an ENSO-induced tropical Indian Ocean-Philippine Sea convection teleconnection pattern, in which the Indian Ocean SSTs warming prevails until summer (Li et al. 2008; Song and Zhou 2014). This warming creates a response in tropospheric temperature through a Matsuno–Gill-type mechanism (Matsuno 1966; Gill 1980), in which a tropospheric Kelvin wave propagates into the equatorial western Pacific and suppresses the convection over the Philippine Sea (Xie et al. 2009, 2016).

Models show strong biases in the ENSO teleconnection paths to EASM (Fu and Lu 2017). Fu et al. (2013) found that some CMIP3 coupled general circulation models (CGCMs) represent ENSO's impact over the EA summer precipitation only when the variability of ENSO is overestimated. However, CGCMs are likely to improve the representation of atmosphere-ocean interactions over the west Pacific and the Indian Ocean for the ENSO teleconnection paths to EASM (e.g., Ding et al. 2014; Fu and Lu 2017), compared with AGCMs (e.g., Wu et al. 2006; Song and Zhou 2014). Although there are signs of improvement in EASM biases in the latest generation of models, most systematic errors have defied years of investment in model development (Sperber et al. 2013).

The effects of the Indian Ocean Dipole (IOD; Saji et al. 1999) on the EASM variability have also been studied. The IOD is an interannual mode of variability characterised by opposing SST anomalies in the western and eastern tropical Indian Ocean. The positive (negative) IOD is linked to a normal (late) EASM onset in the following year (Yuan et al. 2008). A summer following a positive (negative) IOD episode shows an enhanced (weakened) 500-hPa western Pacific subtropical high and an anomalous westwards (eastwards) high ridge. In climate models, the representation of the IOD strength and phases is challenging due to the existent biases in SSTs, and in thermocline and wind feedbacks (Weller and Cai 2013; Ha et al. 2017; Wang et al. 2017). Most CMIP3 and CMIP5 models show that the IOD biases are led by a too-strong Bjerknes feedback simulated in the equatorial Indian Ocean (Cai and Cowan 2013). These biases are caused by a too-strong climatological easterly wind on the east side of the IOD, which leads to an unrealistic thermocline and a largely biased west-to-east SST gradient.

Previous studies have employed the MetUM atmosphere model coupled with a mixed-layer ocean model (Hirons et al. 2015) to understand the effect of global and regional SST biases in Asian rainfall. Using this numeric approach, Levine et al. (2021) identified the strengthening of the atmospheric Indian monsoon base state due to SST biases in the Indian Ocean. Even more, their regional coupled simulations showed to be affected by both differences in SST biases and interannual SST variability. Using MetUM coupled simulations, Stephan et al. (2019) identified the causes of decadal variability of the Silk Road pattern (SRP) teleconnection. These coupled experiments allowed testing the impact of simulated Atlantic and Pacific SST

internal variability: on decadal time scales, the North Atlantic and the North Pacific might indirectly affect the SRP by modulating South Asian rainfall.

This study aims to identify the causes of model errors in simulating the EASM rainfall with a MetUM atmosphere-ocean coupled configuration while using hybrid configurations of the ocean mean state for specific oceanic basins in long-range simulations. Our study aims to identify the effects of global and isolated regional SST biases on the EASM within a coupled-model framework. Relatively novel, this hybrid configuration technique is used for the first time to diagnose the change in EASM systematic errors between simulations, revealing how regional SST biases affect the EASM identifying priority regions for model development to reduce these biases. Also, we identify errors in representing key coupled modes of interannual variability, such as ENSO and the IOD. Using this approach, we investigate errors in mean EASM rainfall, the position of EASM circulation features, such as the WNPSH, and errors in moisture sources and transport pathways for the EASM. The latter is crucial to understand the links between biases in SSTs, evaporation, atmospheric circulation, and convection.

This paper is structured as follows. Section 2 introduces the model simulations, observational and reanalyses data, and analysis methods. Next, results from numerical simulations and analysis of the mean climate and teleconnections are discussed in Sect. 3. Finally, Sect. 4 is a discussion and summarises the main findings of our study.

2 Data and methods

2.1 Met Office global coupled simulation

We analyse output from a climate simulation of an atmosphere-ocean coupled MetUM configuration at the fixed scientific configuration Global Coupled 3.0 (MetUM-GC3; Williams et al. 2017), which comprises Global Atmosphere 7.0 (MetUM-GA7; Walters et al. 2019) coupled to the Nucleus for European Modelling of the Oceans (NEMO) dynamical ocean model. MetUM-GA7 has a horizontal resolution is 1.875° × 1.25° (N96) with 85 vertical levels and a model lid at 85 km. NEMO uses a tri-polar horizontal grid with an approximate resolution of 0.25° with 75 levels unequally spaced in the vertical to provide higher resolution in the upper ocean.

We analyse 100 years (nominally 2013–2112) of the MetUM-GC3 present-day control simulation (GC3), which has fixed greenhouse gases and aerosol concentrations held at approximately 1990 values.

2.1.1 Met Office global ocean mixed layer model experiments: effect of global and regional SST

To understand the effect of MetUM-GC3 SST biases on the EASM, we perform and analyse a set of 30-year climate simulations with the MetUM Global Ocean Mixed Layer 3.0 scientific configuration (MetUM-GOML3). MetUM-GOML3 comprises the same MetUM-GA7 atmosphere as in MetUM-GC3 but coupled to the Multi-Column *K* Profile Parameterisation mixed-layer ocean model in lieu of the NEMO dynamical ocean model. Since MetUM-GOML3 lacks oceanic dynamics, the effects of the mean ocean dynamics on the vertical and horizontal distributions of ocean temperature and salinity are prescribed through temperature and salinity corrections (Hirons et al. 2015; Peatman and Klingaman 2018). These corrections also account for biases in atmosphere-ocean surface fluxes that cause the mean states of coupled models with dynamical oceans to drift. For runs constrained to a single annual climatology, the corrections are computed by first running a ten-year MetUM-GOML3 simulation in which the ocean temperature and salinity are relaxed with a 15-day timescale to a chosen ocean temperature and salinity climatology. For runs constrained to an ENSO or IOD cycle, the relaxation simulations are 30 years long. The daily relaxation terms are saved over the simulation; the mean seasonal cycle of those relaxation terms is then prescribed in the fully coupled simulation, which is run without relaxation. The temperature and salinity corrections are sufficient to constrain the MetUM-GOML3 mean state to the target climatology while still permitting coupled atmosphere-ocean variability on all temporal scales. A significant advantage of MetUM-GOML3 for this study is that the model lacks coupled modes of natural variability, such as ENSO, which often complicate the interpretation of systematic errors in the mean state of coupled models. For further details on MetUM-GOML and the correction method, see Hirons et al. (2015).

We perform and analyse five 30-year MetUM-GOML3 experiments, each to a different ocean mean state. The first, a control experiment (GOML3-OBS), is constrained to an observation-based global ocean climatology: 1980–2009 mean seasonal cycle of the ocean temperature and salinity dataset (Smith and Murphy 2007, hereafter SM07). The second (GOML3-GC3gbl) is constrained to the global ocean mean state from MetUM-GC3. Comparing GOML3-GC3 to GOML3-OBS shows the effect of global MetUM-GC3 mean SST biases. Importantly, MetUM-GOML3 allows the effects of these coupled-model SST biases to be reproduced in a (thermodynamic) coupled model configuration rather than the traditional experiment design of using atmosphere-only models with prescribed coupled-model SSTs. The final set of three experiments are constrained hybrid configurations of the observed and the MetUM-GC3 ocean mean states,

with the MetUM-GC3 mean state imposed in only one ocean basin: only in the Atlantic Ocean (GOML-GC3atl), only in the Pacific Ocean (GOML3-GC3pac) and only in the Indian Ocean (GOML3-GC3ind). Comparing any of these experiments to GOML3-OBS shows the effect of biases in the target ocean basin, again in an air-sea coupled model configuration. The experiments are summarised in Table 1.

These five MetUM-GOML3 experiments are run for 30 years each, initialised from the end of the corresponding ten-year relaxation simulation. All MetUM-GOML3 simulations in this paper use the exact N96L85 atmospheric resolution as in MetUM-GC3. The atmospheric and oceanic resolutions are identical as GOML3 runs with one mixed-layer ocean column under each atmospheric gridpoint. The GOML3 ocean has 100 vertical points in a 1000 m column, unevenly spaced to provide finer resolution in the upper ocean.

2.1.2 Met Office global ocean mixed layer model experiments: effect of global SST on ENSO and IOD teleconnections on the EASM

MetUM-GOML also permits simulations where the SST variability from a large-scale climate mode (e.g., ENSO or the IOD) is added to the ocean mean state as a repeating multi-annual cycle. The effect of MetUM-GC3 SST biases on ENSO and IOD teleconnections to the EASM is investigated. For this, we perform and analyse four 60-year MetUM-GOML3 experiments, each constrained to a different combination of mean state and variability. The first, a control experiment (GOML3-OBS_ENSO), is constrained to an observation-based global ocean climatology of the SM07 dataset and a 3-year repeating observed ENSO cycle (e.g., a 3-year-repeating cycle of El Niño, La Niña and neutral conditions; Klingaman and Demott 2020). The second (GOML3-GC3_ENSO) is constrained to a hybrid configuration of the global ocean mean state from MetUM-GC3 and a 3-year repeating observed ENSO cycle. The comparison of GOML3-GC3_ENSO to GOML3-OBS_ENSO shows the effect of global MetUM-GC3 mean SST biases on the representation of the ENSO teleconnection in GOML3.

The third is a control experiment (GOML3-OBS_IOD) is constrained to an observation-based global ocean climatology of the SM07 dataset and a 3-year repeating observed IOD cycle (a 3-year-repeating cycle of positive IOD phase, negative IOD phase, and neutral conditions). Finally, the fourth experiment (GOML3-GC3_IOD) is a constrained hybrid configuration of the global ocean mean state from MetUM-GC3 and a 3-year repeating observed IOD cycle. The differences between GOML3-OBS_IOD and GOML3-GC3_IOD reveal how biases in the GC3 ocean mean state affect the teleconnections of the IOD to the EASM, separate from the effects of biases in the GC3 representations of IOD itself. The experiments are summarised in Table 2. For these analyses, the MetUM-GOML3 experiments are run for 60 years, initialised from the end of the corresponding 30-year relaxation simulation.

Table 3 indicates the purpose of the comparison among the experiments detailed in Sect. 2 and helps to interpret the highlights of the effect of global and regional GC3 SST biases.

2.2 Water Accounting Model-2layers

The Water Accounting Model-2layers (WAM-2layers; van der Ent et al. 2013, 2014) is an Eulerian moisture tracking method based on the atmospheric water conservation

Table 1 Key to MetUM and MetUM-GOML3 experiments performed and analysed in Sects. 3.2 and 3.3, including the name used in the text and the ocean mean state to which the simulation is constrained

Simulation	Ocean mean state
MetUM-GC3	MetUM-GC3 globally
GOML3-OBS	SM07 (observed climatology) globally
GOML3-GC3gbl	MetUM-GC3 globally
GOML3-GC3atl	MetUM-GC3 in Atlantic, SM07 (observed climatology) elsewhere
GOML3-GC3ind	MetUM-GC3 in Indian, SM07 (observed climatology) elsewhere
GOML3-GC3pac	MetUM-GC3 in Pacific, SM07 (observed climatology) elsewhere

Table 2 Key to MetUM-GOML3 experiments performed and analysed in Sects. 3.4.1 and 3.4.2, including the name used in the text and the ocean mean state to which the simulation is constrained

Simulation	Ocean mean state
GOML3-OBS_ENSO	SM07 + 3-year repeating observed ENSO cycle
GOML3-GC3_ENSO	MetUM-GC3 + 3-year repeating observed ENSO cycle
GOML3-OBS_IOD	SM07 + 3-year repeating observed IOD cycle
GOML3-GC3_IOD	MetUM-GC3 + 3-year repeating observed IOD cycle

Table 3 Set of MetUM-GOML3 experiments performed and analysed in Sects. 3.2, 3.3, and 3.4, and the result of the comparison with each other

Experiments confronted	Result of the comparison between the two experiments
GOML3-GC3gbl vs. GOML3-OBS	The effect of global MetUM-GC3 mean SST biases
GOML3-GC3atl vs. GOML3-OBS	The effect of Atlantic MetUM-GC3 mean SST biases
GOML3-GC3ind vs. GOML3-OBS	The effect of Indian MetUM-GC3 mean SST biases
GOML3-GC3pac vs. GOML3-OBS	The effect of Pacific MetUM-GC3 mean SST biases
GOML3-GC3_ENSO vs. GOML3-OBS_ENSO	The effect of global MetUM-GC3 mean SST biases on the ENSO teleconnection
GOML3-GC3_IOD vs. GOML3-OBS_IOD	The effect of global MetUM-GC3 mean SST biases on the IOD teleconnection

equation, that traces moisture sources or sinks using a combination of precipitation, evaporation, and moisture flux from a chosen domain. In this study, we apply the WAM-2 layers to trace atmospheric moisture from origin to destination or vice versa. We use the WAM-2layers output variable that represents the tracked evaporation, which means the evaporation from any grid point (globally) that becomes precipitation in a defined study region (box). In addition, this variable defines the source regions that represent the sum of tracked evaporation equal to the precipitation in the study region (box).

The region of study for the WAM-2layers analysis is enclosed by 20°–33° N latitude and 105°–124° E longitude, and is referred to as the "South China box" onwards. The WAM-2layers has been successfully applied by Guo et al. (2019) and Guo et al. (2020) to track sources or sinks of moisture related to East Asian precipitation simulated with GOML3. In this study, we apply the WAM-2layers to the fifth-generation European Centre for Medium-Range Weather Forecasts reanalysis (ERA5; Hersbach et al. 2020) reanalysis, the experiments GOML3-GC3gbl, GOML3-OBS, GOML3-GC3ind, GOML3-GC3pac and GOML3-GC3atl (see Table 1 for reference), and all the GOML3 experiments for ENSO and IOD cycles described in Table 2.

2.3 Validation datasets

In Sect. 3, we compare simulated rainfall to rainfall from ERA5 reanalysis and the version-2 Global Precipitation Climatology Project (GPCP; Adler et al. 2018), available for 1979–2019. ERA5 rainfall dataset is used for consistency with the WAM analysis described in Sect. 2.2. Jiao et al. (2021) found that ERA5 captures the annual and seasonal patterns of rainfall in China, though slightly overestimates precipitation during summer. Nogueira (2020) showed that, using the GPCP data as a reference, ERA5 has a good representation of rainfall over southeast Asia, improving the performance of its predecessor, the ERA-interim reanalysis (Dee et al. 2011). The author suggests ERA5 better represents tropical circulation, deep convection intensity, and moisture flux convergence patterns. In the present study, we also compare simulated winds to those from ERA5, available for 1979–2019. Simulated sea surface temperature (SSTs) are compared to observations from the National Oceanic and Atmospheric Administration (NOAA), fifth-version of the Extended Reconstructed Sea Surface Temperature product (ERSSTv5; Huang et al. 2017), available for 1979–2019. All validation data are interpolated onto the MetUM N96 grid using the area-weighted interpolation. Linear regression analysis and/or the statistical hypothesis test (t-test) are used to analyse the experiments presented in this study.

3 Results

3.1 GC3 rainfall biases

In this section, we assess the representation of rainfall over East Asia in the MetUM-GC3 present-day control simulation (MetUM-GC3), comparing it to ERA5 rainfall and GPCP rainfall (1979–2019). MetUM-GC3 presents a delayed northward progression of rainfall (in July rather than in June), as well as too little northward propagation when it does happen (to ≈ 30–35° N rather than ≈ 40° N). The withdrawal occurs too early (in early August rather than mid-August and September; figure not shown). During June-September (JJAS), GC3 underestimates rainfall over east China, the Korean Peninsula, and the Sea of Japan, with biases up to -3 mm day^{-1}, whereas rainfall is overestimated in south-eastern China, with biases up to $+5$ mm day^{-1} (Fig. 1). Positive biases of rainfall are also found in most of the Indochinese Peninsula, the South China Sea, and the Philippine Sea, which indicates a systematic misrepresentation of the northward progression of the EASM in GC3. The strongest GC3 dry bias is found in most of the Maritime Continent, the Bay of Bengal, and India, with underestimations of rainfall of up to 11 mm day^{-1}.

3.2 Effects of global GC3 SST biases on EASM using GOML3

In this section, we compare the GOML3 simulation constrained to the GC3 ocean mean state (GOML3-GC3gbl)

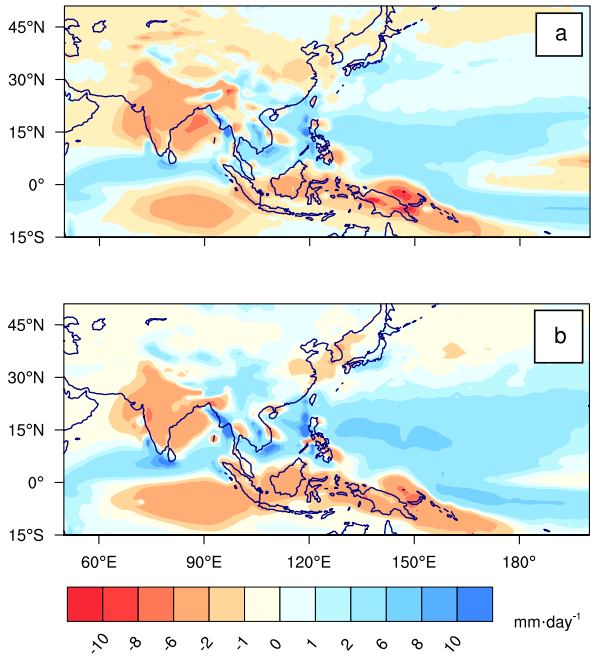

Fig. 1 Rainfall bias of MetUM forced by the GC3 global ocean mean state, during JJAS, from **a** MetUM-GC3 minus ERA5 reanalysis rainfall, and **b** MetUM-GC3 minus GPCP rainfall (mm day^{-1})

with the GOML3 simulation constrained to the observed ocean mean state (GOML3-OBS) to show the effect of GC3 SST systematic errors on the EASM. This comparison indicates that GC3 global SST biases, when taken together, have little effect on the JJAS mean rainfall and circulation in the EASM region (Fig. 6d). However, the negligible seasonal mean differences hide a substantial shift in the seasonal cycle. GC3 SST biases delay the onset of the monsoon over southern China, reducing rainfall in June and increasing rainfall in July (Fig. 2). GC3 global SST biases also reduce rainfall in August and increase rainfall in September, perhaps because the monsoon retreats later across southern China in GOML3-GC3gbl than in GOML3-OBS. These differences are associated with an anomalous anticyclonic circulation in the West Pacific near the Philippines, corresponding to an enhanced WNPSH. As a result, convection over the West Pacific shifts south and east, reducing the overestimated South China Sea rainfall in atmosphere-only simulations (GC3 experiment). This shift is associated with a quadrupole pattern of rainfall differences, with centres over the equatorial Indian Ocean, India, north of the Maritime Continent and the West Pacific (Fig. 3).

The GC3 global SST biases delay the EASM northward progression over continental China, enhancing vertically integrated moisture transport (VIMF) divergence over a large portion of southeastern China and southern Japan in June (not shown). On the other hand, VIMF convergence is enhanced in the Pacific portion of the sea located around the Ryukyu Islands region. In June, GC3 SST biases increase the outgoing long-wave radiation (OLR; not shown) over southeastern China, India, Bangladesh and most of the Indian Ocean, associated with reduced deep convection and rainfall (Fig. 3). Conversely, GOML3-GC3gbl strongly increases convective activity and rainfall in the Maritime Continent and, to a lesser extent, the North Pacific Ocean.

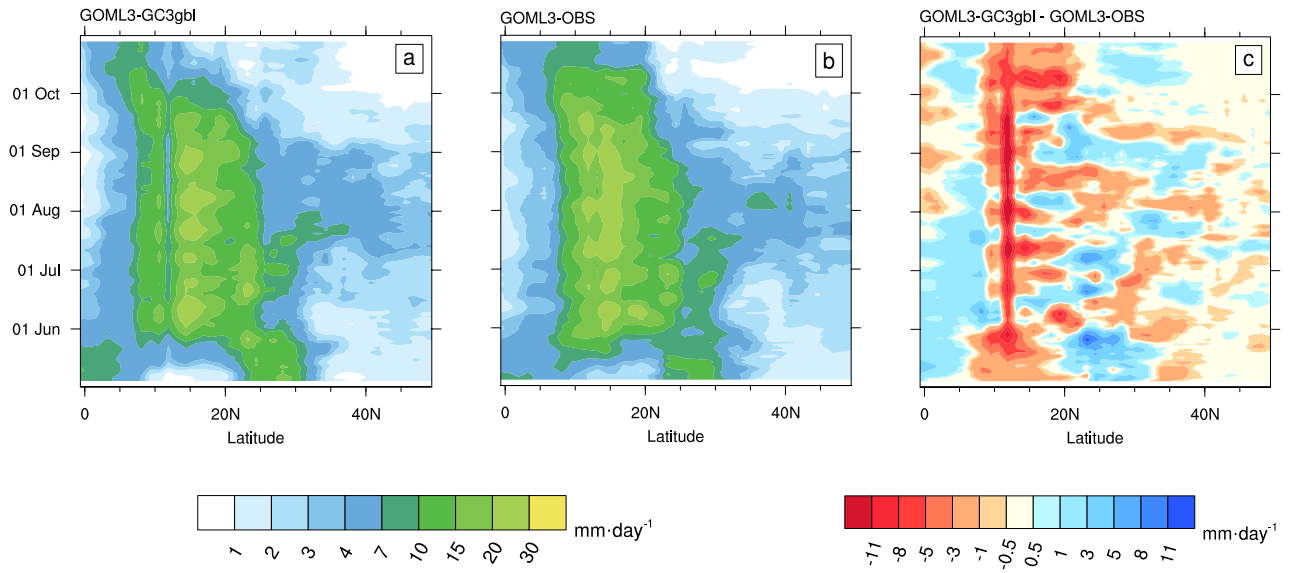

Fig. 2 Time vs. latitude Hovmöller diagrams of 115°–122° E averaged rainfall (mm day^{-1}) for **a** GOML3-GC3gbl, **b** GOML3-OBS experiments, and **c** the difference between them (GOML3-GC3gbl minus GOML3-OBS)

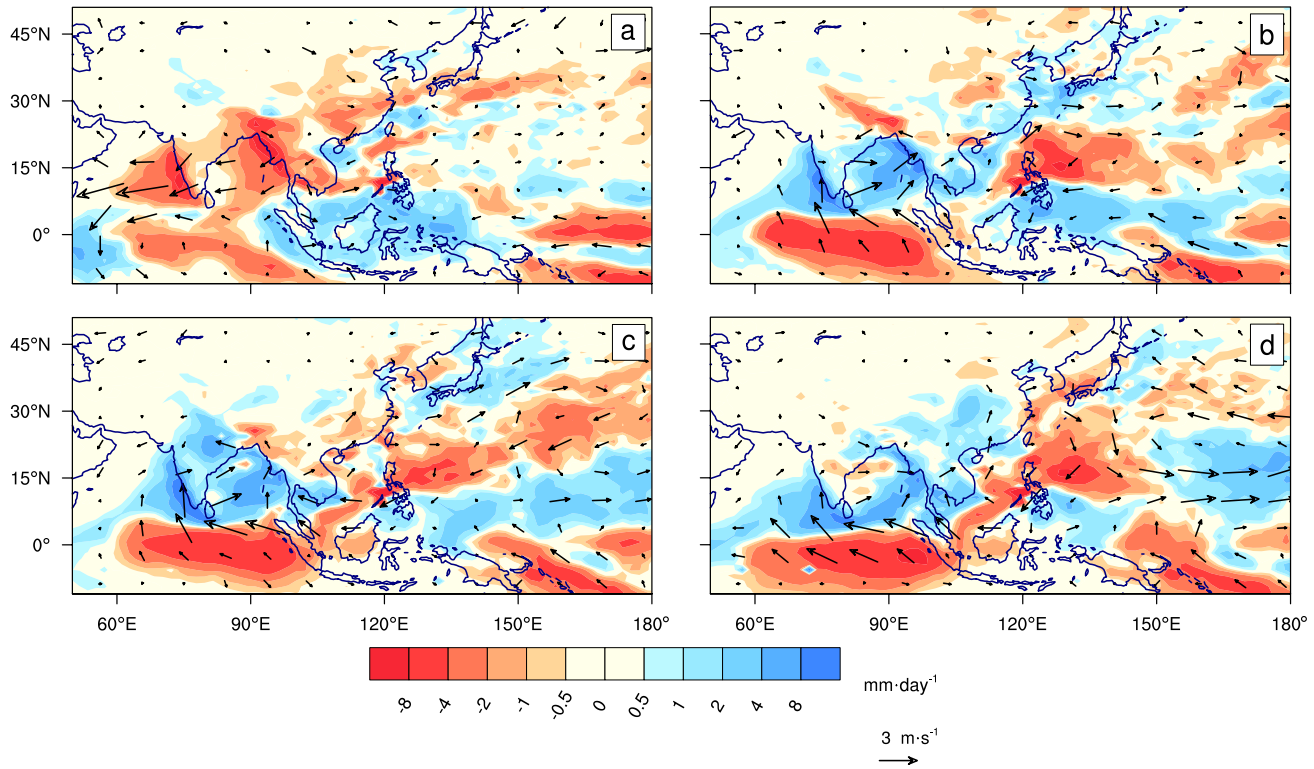

Fig. 3 Effect of GC3 global SST biases used to force the GOML3 model in the GOML3-GC3gbl experiment on **a** June, **b** July, **c** August, and **d** September rainfall (shaded, mm day^{-1}) and on 850 hPa winds (arrows, m s^{-1})

As the EASM season progresses, GC3 global SST biases promote a quadrupole pattern of rainfall and convection differences that prevail through the rest of the monsoon season (Fig. 3). The two left-side poles of this quadrupole are characterised by enhanced precipitation in India and Bangladesh (upper pole) and reduced precipitation over the equatorial Indian Ocean (down pole). In addition, differences in 850 hPa winds indicate an enhanced Indian monsoon circulation (Fig. 3).

In September, a late retreat of the EASM is associated with increased deep convection and rainfall over southeast China and the Indochinese Peninsula and reduced rainfall over the Philippine Sea and most of the Maritime Continent.

We compute the moisture sources for June-September rainfall in an area of South East China with strong differences between simulated and observed rainfall, which is enclosed by the South China box (Fig. 4). The South China box corresponds to most South East China and resembles Region 1 in Guo et al. (2019). We determine moisture sources of precipitation over EA in both ERA5 reanalysis and GOML3 experiments using the WAM-2layers method, described in Sect. 2.2.

Through the EASM season, most of the differences between GOML3-GC3gbl and GOML3-OBS are found in the Philippine Sea, the Arabian Sea, the Indian Ocean, Southern China, and the Tibetan Plateau (Fig. 4). The differences of moisture sources of rainfall in the south China box reach up to ± 6 mm day^{-1}, where GC3 negative differences are found in the Philippine Sea throughout the season. During June, the GC3 simulations underestimate moisture sources of rainfall over the Indian Ocean and the Indochinese peninsula. Simultaneously, the GC3 anomalies present weakened vertically integrated moisture flux over the Indian Ocean, related to a weakened Indian monsoon circulation (Fig. 4a). Rodríguez et al. (2019) suggested that mid-June dry biases over the Indian peninsula and the Bay of Bengal are linked to an erroneous Hadley circulation that connects biases of the West Pacific's convergence with the Maritime continent divergence.

As the EASM season progresses, the moisture flux anomalies turn to follow an enhanced Indian monsoon circulation (Fig. 4b). At the end of the monsoon season (September), the largest GOML3-GC3gbl overestimates of moisture are present in South China, the Tibetan Plateau, and the Indochinese Peninsula (Fig. 4c), with up to $+6$ mm day^{-1}, which is associated with the late withdrawal of the EASM.

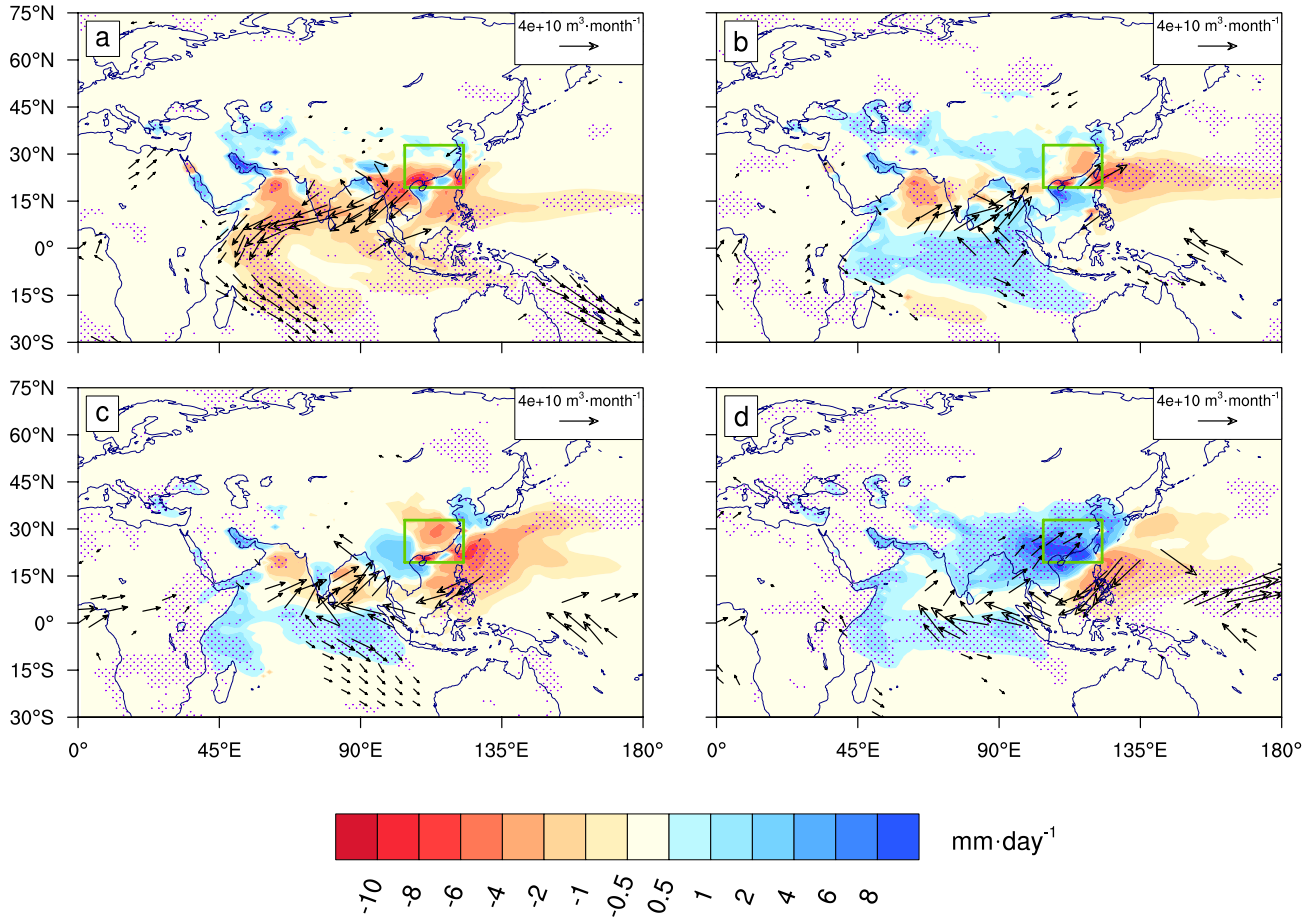

Fig. 4 Difference in the WAM-2layers tracked mean moisture source for the precipitation in south China box delimited by the green polygon (shaded, mmday^{-1}) and tracked vertically integrated moisture flux (vectors, m^3 month^{-1}), calculated with GOML3 with global SST bias (GOML3-GC3gbl) minus GOML3 with observed SSTs (GOML3-OBS) for **a** June, **b** July, **c** August, and **d** September. Stippling and vectors indicate significance at the 5% level using the Student's t-test

3.3 Effects of regional GC3 biases on EASM using GOML3

We further explore the mechanisms by which GC3 SST biases influence the EASM by using GOML3 simulations to isolate the effects of regional GC3 SST biases in the Indian, Pacific, and Atlantic Oceans. We compare GOML3-GC3ind, GOML3-GC3pac and GOML3-GC3atl, respectively, to GOML3-OBS and results are shown in Figs. 5 and 6.

The GC3 Indian Ocean SST biases are characterised by cold SSTs in the northern Indian Ocean (Fig. 5a). These SST biases reduce JJAS rainfall by up to 2 mm day^{-1} over most southeastern China and the East China Sea (Fig. 6a), linked to an anomalous cyclonic upper-tropospheric circulation at 200 hPa near ≈ 32° N.

GC3 Indian Ocean SST biases cause a dipole pattern of precipitation anomalies with enhanced rainfall over India and the Bay of Bengal and suppressed rainfall in the equatorial Indian Ocean. This is related to an enhanced Indian monsoon circulation, which prevails most of the summer. These cold SST biases have been found in studies using previous configurations of the MetUM (e.g., Levine and Turner 2012; Levine et al. 2021) and have been attributed to errors in atmospheric wind stress forcing of the Indian Ocean. The WAM-2layer analysis for GOML3-GC3ind experiments shows that the reduction of rainfall in the south China box is associated with cyclonic moisture transport difference centred over continental India (Fig. 7a). This decrease in rainfall is also related to negative moisture sources of rainfall in the Indian Ocean and the Philippine Sea, with up to −2 mm day^{-1} in both cases.

Cold SSTs characterise the GC3 SST biases in the Pacific Ocean in most of the North Pacific and warm SSTs in the extratropical South Pacific (Fig. 5b). These SST biases are linked with an anomalous 850 hPa anticyclone centred in the North Pacific. Simultaneously, the mean flow in the East

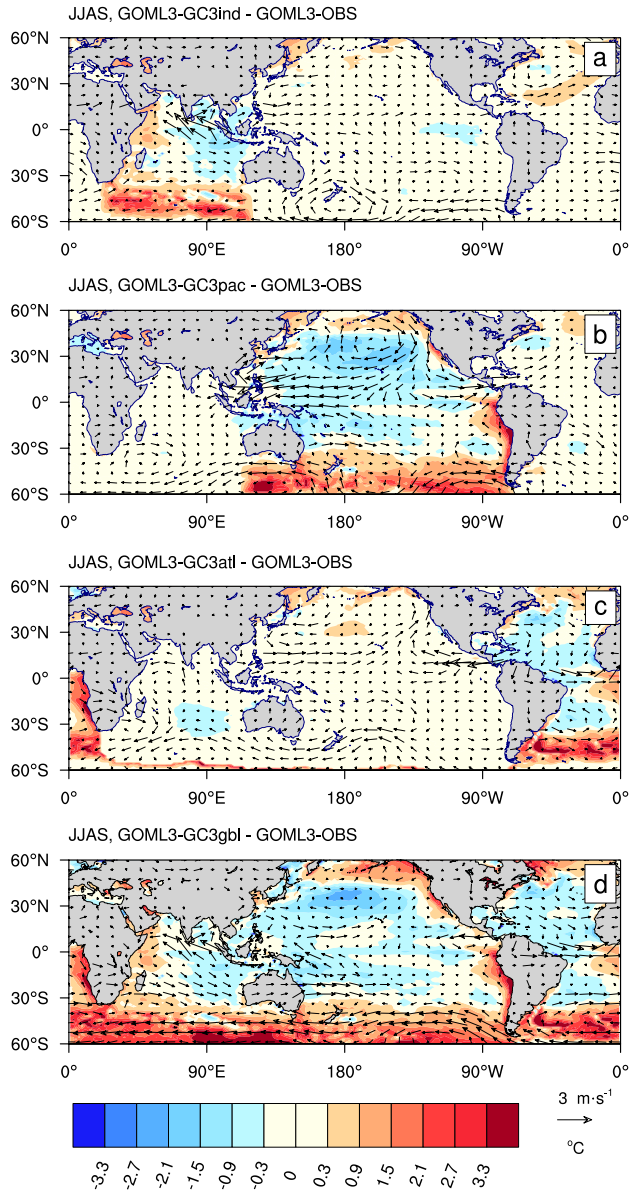

Fig. 5 Differences in JJAS SSTs (shaded, °C) and 850 hPa winds (arrows, m s^{-1}) for **a** GOML3-GC3ind minus GOML3-OBS, **b** GOML3-GC3pac minus GOML3-OBS, **c** GOML3-GC3atl minus GOML3-OBS, and **d** GOML3-GC3gbl minus GOML3-OBS experiments

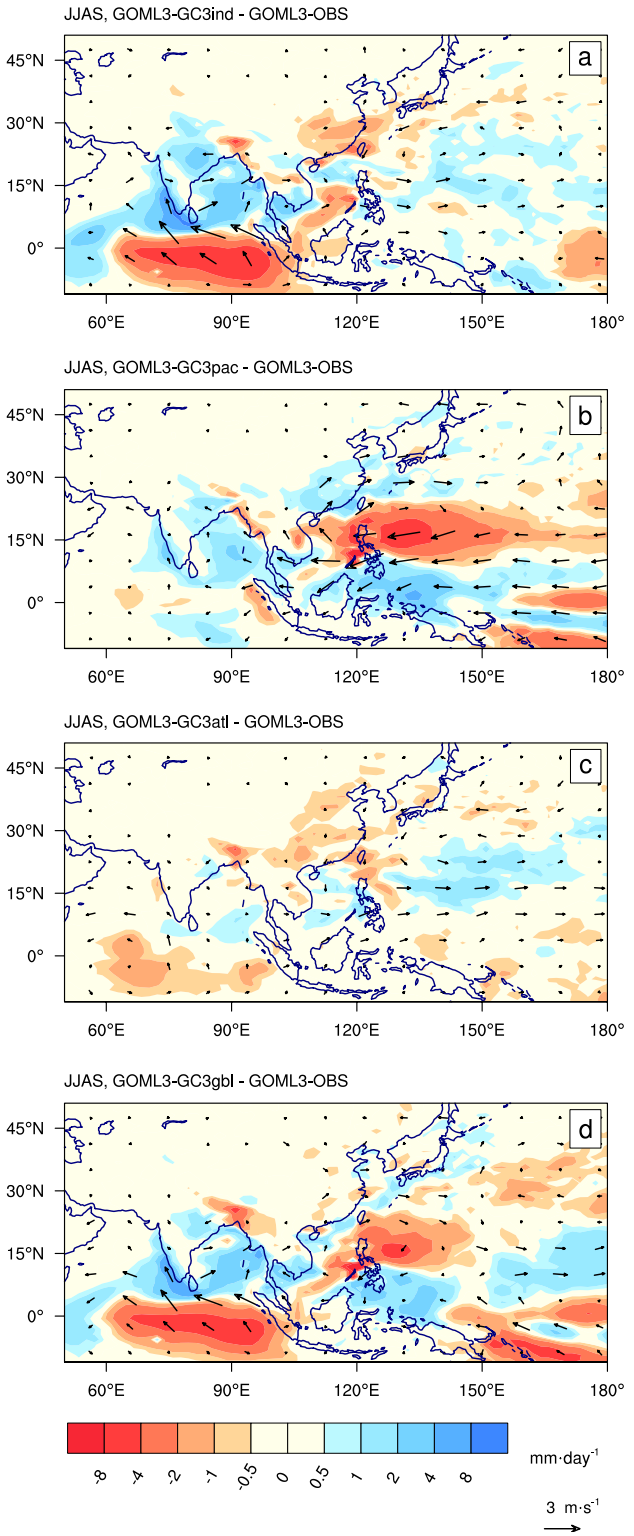

Fig. 6 Differences in JJAS rainfall (shaded, mm day^{-1}) and 850 hPa winds (arrows, m s^{-1}) for **a** GOML3-GC3ind minus GOML3-OBS, **b** GOML3-GC3pac minus GOML3-OBS, **c** GOML3-GC3atl minus GOML3-OBS, and **d** GOML3-GC3gbl minus GOML3-OBS experiments

Pacific, the Caribbean Sea and the North Atlantic subtropical high circulation weaken. This link between the large-scale features of the two oceans is known as the 'atmospheric bridge', which links the Hadley and Walker circulations in the Pacific with the Atlantic Hadley circulation (e.g., Alexander and Scott 2002).

Regionally, the GC3 Pacific SST biases strengthen the WNPSH centred in the Philippine Sea (Fig. 5b) and increase seasonal rainfall over most of southeastern China. This is

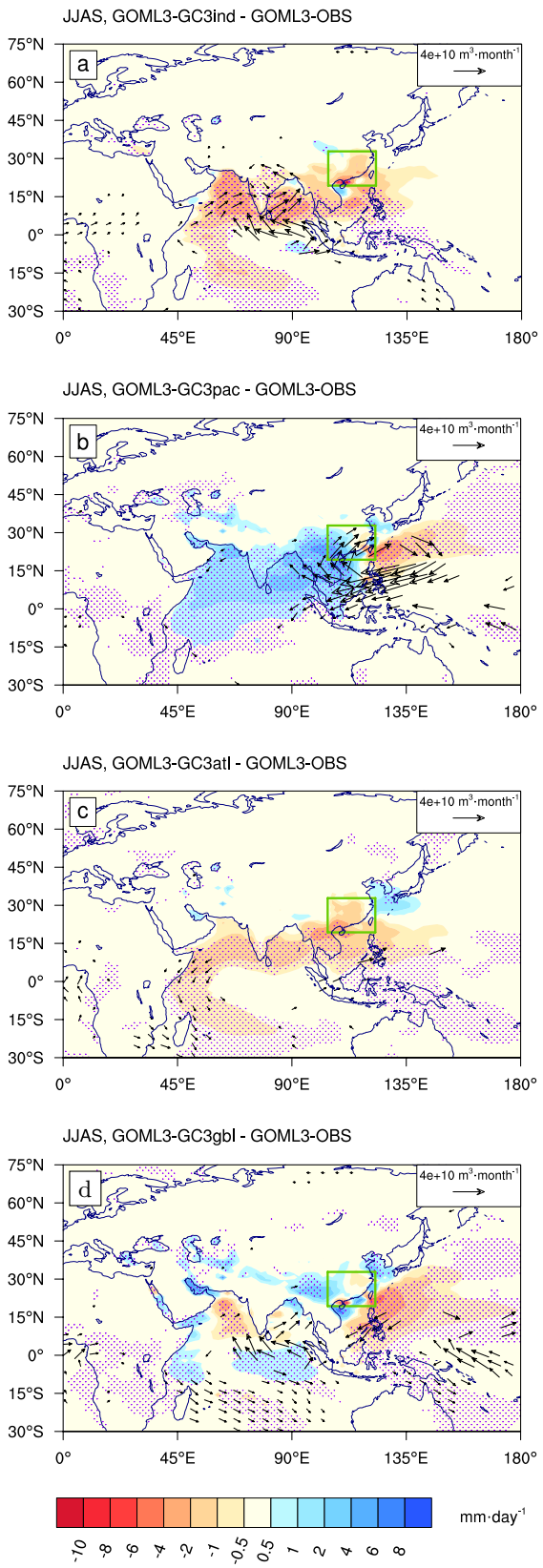

Fig. 7 Differences in the JJAS moisture sources of rainfall (shaded, ▶ mmday^{-1}) and vertically integrated moisture transport (arrows, m^3 month^{-1}), obtained using the WAM-2layers for the South China box (green box) for **a** GOML3-GC3ind minus GOML3-OBS, **b** GOML3-GC3pac minus GOML3-OBS, **c** GOML3-GC3atl minus GOML3-OBS, and **d** GOML3-GC3gbl minus GOML3-OBS experiments. Stippling and vectors indicate significance at the 5% level using the Student's t-test

related to an earlier northward progression of the EASM in June, characterised by a prominent band of enhanced rain around 20–30° N, which extends over China and the East China Sea, with up to 2–4 mm day^{-1} more rainfall (Fig. 6b). On the other hand, the Pacific SST biases suppress rainfall in the South China and the Philippine Seas and increase rainfall in the equatorial Pacific and the southern Maritime Continent.

The GC3 Pacific Ocean SST biases increase rainfall over India and the Bay of Bengal during July and August, with up to +4 mm day^{-1} more precipitation (Fig. 6b). These increases in rainfall are related to an anomalously enhanced monsoonal circulation that intensifies convective activity in South East China. However, the influence of the Pacific Ocean SST biases on Indian monsoon rainfall is less pronounced than that of Indian Ocean SST anomalies. A last retreat of the EASM in September increases rainfall in most of southeast China, Bangladesh, and the Bay of Bengal (not shown). On the other hand, the later monsoon retreat reduces rainfall over the southern China Sea, extending towards the Philippine Sea.

The WAM-2layer analysis applied to the GOML3-GC3pac experiment shows an anticyclonic moisture transport difference centred over the Philippine Sea, which is associated with the increase of rainfall in the south China box region during JJAS (Fig. 7b). This decrease in rainfall is also associated with differences in moisture sources of rainfall with up to +4 mm day^{-1} in the Indian Ocean, and −4 mm day^{-1} the western Pacific.

GC3 Atlantic SST biases show wide-basin cold biases, except the extratropical latitudes and the South Atlantic near Africa (Fig. 5c). The effect of GC3 Atlantic SST biases in JJAS is characterised by a dipole of suppressed and enhanced rainfall between southeast China and the North Pacific, respectively (Fig. 6c). These SST biases are associated with an anomalously enhanced low-level mean flow in the East Pacific and a weaker North Pacific subtropical high circulation. The anomalous circulations are related to reduced JJAS rainfall over most of southeast China by up to 2 mm day^{-1}.

The WAM-2layers analysis applied to the GOML3-GC3atl experiment shows that the reduced JJAS rainfall in the south China box is associated with a reduction of moisture sources of rainfall in the Indian Ocean, the Indochinese Peninsula and the Philippine Sea (Fig. 7c)

In summary, the three GOML3 simulations mentioned above (GOML3-GC3atl, GOML3-GC3ind, and GOML3-GC3pac) allow us to distinguish the effect of regional GC3 SST biases on the EASM. While the Indian and the Atlantic SST biases cause dry conditions in southeast China by up to -2 mm day^{-1} (Fig. 6a, c, respectively), the Pacific SST biases cause wet conditions by up to 2 mm day^{-1} in most of southeast China during JJAS (Fig. 6b). The sum of these three regional SST biases results in rainfall differences between ± 0.5 mm day^{-1} in most of southeast China, as seen in the GOML3-GC3glb simulation (Fig. 6d).

3.4 Errors in ENSO and IOD teleconnection pathways to EASM

This section aims (a) to assess the simulated EASM teleconnections from near-perfect ENSO and IOD events, given that GOML3 has small biases in the mean state and includes ENSO and IOD cycles derived from observations; and (b) to understand how GC3 mean-state SST biases affect the representation of the ENSO and IOD teleconnections to the EASM.

3.4.1 ENSO

To analyse errors in the ENSO teleconnection pathways to the EASM, we linearly regress GOML3-OBS_ENSO and GOML3-GC3_ENSO simulated seasonal meteorological variables onto the standardised season-and-area-averaged SSTs for the Niño 3.4 region. Similarly, for observational comparison, we compute linear regressions of season-and-area-averaged SSTs of ERSSTv5 and ERA5 meteorological variables onto ERSSTv5 SSTs for the Niño 3.4 region.

First, we examine JJAS SSTs regressions and winds at 850 hPa (Fig. 8). In all cases, the regressions show the SSTs and low-level wind anomalies typical of a developing central Pacific El Niño. The main difference between the regressed SST for ERSSTv5 and GOML3 experiments is found in the easternmost equatorial East Pacific, where ERSSTv5 SST regressions reach about 1 °C anomalies. Both GOML3 significant regressed SSTs get anomalies up to 0.3 °C; this may occur due to the lack of variability in GOML since observed SST variability is driven by ocean dynamics, which GOML cannot simulate (e.g., Hirons et al. 2015; Levine et al. 2021). Although not statistically significant, ERSSTv5 and both GOML3 regressions also show differences in the SST magnitude in the Indian Ocean. While ERSSTv5 reaches up to 0.3 °C in a large portion of the Arabian Sea and the equatorial Indian Ocean, SSTs in both GOML3 simulations reach up to 0.05 °C.

During JJAS, ERA5 and GOML3 regression analyses show that western Pacific anomalous equatorial westerly

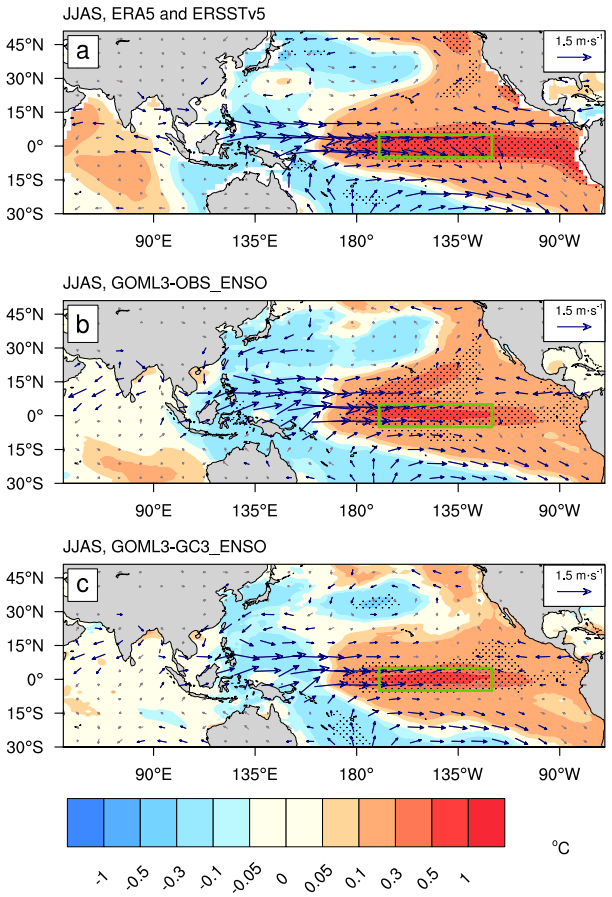

Fig. 8 Mean JJAS SSTs (shaded, °C) and winds at 850 hPa (arrows, ms^{-1}) regressed onto standardised JJAS Niño 3.4 SSTs for **a** ERA5 and ERSSTv5, **b** GOML3-OBS_ENSO, and **c** GOML3-GC3_ENSO. Stippling indicates SSTs significant at the 5%. Wind vectors are drawn in navy blue color when at least one of the components of the vector is significant at the 5% level using the Student's t-test. The green box delimits the Niño 3.4 region

winds at 850 hPa positively correlated with ENSO. However, the anomalous westerlies over the West Pacific extend northwards 15° N in both GOML3 experiments (Fig. 9b, c) during JJAS. In both GOML3 experiments, the anomalous westerly winds weaken the WNPSH, centred at ≈ 25° N, 175° E. These cyclonic circulation anomalies extend to continental China. The 850 hPa anomalous circulation is associated with reduced rainfall in South East China in GOML3 experiments. Also, at low levels in the troposphere, both GOML3-OBS_ENSO and GOML3-GC3_ENSO simulations show an anomalous anticyclonic circulation over India and anomalous northeasterlies associated with a weakened Indian monsoon circulation over the northern Indian Ocean in El Niño years (Fig. 9b, c, respectively). These anomalous regional circulations are associated with errors in the signal of anomalous

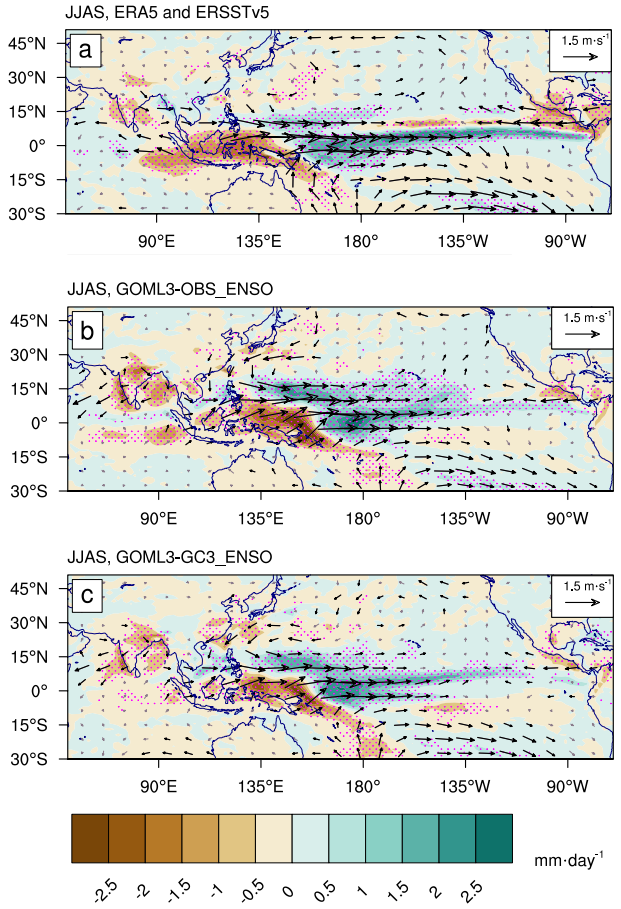

Fig. 9 Mean JJAS rainfall (shaded, mmday^{-1}) and winds at 850 hPa (arrows, ms^{-1}) regressed onto standardised JJAS Niño 3.4 SSTs for **a** ERA5 and ERSSTv5, **b** GOML3-OBS_ENSO, and **c** GOML3-GC3_ENSO experiments. Stippling indicates rainfall significance at the 5% level using the Student's t-test. Wind vectors are drawn in black color when at least one of the components of the vector is significant at the 5% level using the Student's t-test

precipitation simulated over India, the Bay of Bengal, and the Arabian Sea located west of India with GOML3.

JJAS ERA5 regressed winds onto Nino 3.4 suggest that the entire North Pacific Subtropical High (NPSH, centred at ≈ 35° N, 177° E) is weakened during developing El Niño (Fig. 9a). However, the anomalous circulation associated with the NPSH is weaker in GOML3-OBS_ENSO during developing ENSO, and it is centred about 7 degrees further east in GOML3-GC3_ENSO regressions (≈ 35° N, 170° W).

To understand the overall effect of GC3 mean-state errors influencing the ENSO teleconnection to the EASM rainfall, we analyse the GOML3-OBS_ENSO and GOML3-GC3_ENSO regressions. JJAS precipitation anomalies over ≈ 20° − 40° N, simulated with GOML3-OBS_ENSO (Fig. 9b) and GOML3-GC3_ENSO (Fig. 9c), are significantly anticorrelated with Niño 3.4, with up to ≈ −0.5 and ≈ −1 mm day^{-1}, respectively. However, JJAS ERA5 rainfall is significantly anticorrelated with simultaneous SSTs from the Niño 3.4 region (Fig. 9a), only over the northernmost portion of South East China (≈ 30° − 40° N). This regression analysis suggests that during developing El Niño (La Niña) episodes, this area experiences drier (wetter) conditions.

The major biases in the ENSO teleconnection to the EASM rainfall with GC3 are identified when directly comparing GOML3-GC3_ENSO against GOML3-OBS_ENSO rainfall simulations. At the beginning of the EASM season, GOML3-GC3_ENSO presents dry conditions in southeast China, the Bay of Bengal, and the Indochinese Peninsula, during both developing El Niño and La Niña (not shown). Additionally, GOML3-GC3_ENSO presents wet conditions in the Maritime continent. The aforementioned anomalous conditions resemble the ones present in the GOML3-GC3gbl experiment in June (Fig. 3a), implying that these ENSO-teleconnection biases between GOML3-GC3_ENSO simulation are predominately related to GC3 SST biases. In July, GOML3-GC3_ENSO simulations are drier for a large area of southeast China (between ≈ 30° − 40° N) during developing El Niño events (not shown). However, during developing La Niña, GC3 presents more rainfall in most of southeast China. At this point of the simulations, the EASM rainfall does not penetrate northwards enough, implying that GOML3-GC3_ENSO exacerbates the dry conditions during the EASM in northern southeast China during both ENSO phases.

In August, GOML3-GC3_ENSO enhances the Indian Monsoon circulation in both developing ENSO phases, leading to more rainfall in continental India and the Bay of Bengal and less rainfall over the equatorial Indian Ocean (not shown), similar to the ones in the GOML3-GC3gbl experiment in August (Fig. 3c).

Most of the differences in JJAS precipitation between ERA5 and both GOML3 simulations are seen over southernmost South East Asia (≈ 20° − 30° N): while ERA5 rainfall is positively correlated with Niño 3.4 SSTs in southernmost East China and the Indochinese Peninsula (Fig. 9a), GOML3-OBS_ENSO and GOML3-GC3_ENSO are significantly anticorrelated over the region mentioned above (Fig. 9b, c, respectively). These analyses suggest that GOML3 presents a systematic bias of underestimated rainfall in South East China during El Niño years. The GC3 ocean mean state bias exacerbates this error, which affects the ENSO teleconnection to the EASM by simulating drier (wetter) conditions over South East China during El Niño (La Niña) events.

ERA5 and both GOML3 experiments differ in the location of anomalous rainfall along the central Pacific Ocean. While both GOML3 experiments show a significant positive

correlation of rainfall with ENSO, ERA5 shows a negative correlation that extends ≈ 7 – 10° N latitude. This particular feature in ERA5-regressed JJAS rainfall is related to the anomalous equatorward (poleward) shift of the Intertropical Convergence Zone (ITCZ) during El Niño (La Niña) events (e.g., Berry and Reeder 2014), which is not properly captured in either GOML3 experiment.

We investigate the errors in ENSO teleconnection pathways to the EASM and compute the moisture sources for JJAS rainfall in the south China box (defined previously in Sect. 2.2). Figure 10 shows the regressions of moisture sources and moisture transport onto Niño 3.4 SSTs. These regression analyses suggest that ERA5 rainfall in the south China box is positively correlated with moisture sources from continental India, the Arabian Sea, the Bay of Bengal, the south Maritime Continent, and the region of Guizhou and Guangxi in South East China during El Niño. Simultaneously, anomalous northeastwards moisture transport from the Tibetan Plateau and continental India is positively correlated with anomalies of rainfall in the South China box.

GOML3 errors in simulating the moisture sources of rainfall in the south China box are found mainly in the Indian Ocean (Fig. 10), having the opposite sign to the ERA5 regressions. The GOML3 simulations also present a northward bias in the location of moisture transport vectors over the Pacific Ocean. As discussed, the precipitation in the south China box during JJAS is weakened (enhanced) by MetUM GOML3 experiments during El Niño (La Niña). The regression analysis for GOML3 experiments suggests that, during El Niño events, the reduced rainfall in the south China box simulated with GOML3-OBS_ENSO and GOML3-GC3_ENSO is associated with reduced moisture from a large area of the equatorial Indian Ocean, the Bay of Bengal, the Arabian Sea and the Maritime Continent. These regressions also suggest that during El Niño, the reduced rainfall simulated with both GOML3 experiments in the south China box is associated with a weaker moisture transport from the Indian monsoon circulation. In all cases, both GOML3 simulations show opposite conditions during La Niña. The biases with GOML3 precipitation in the south China box come from errors capturing important sources of moisture and moisture transport from the Indian Ocean and the Maritime Continent.

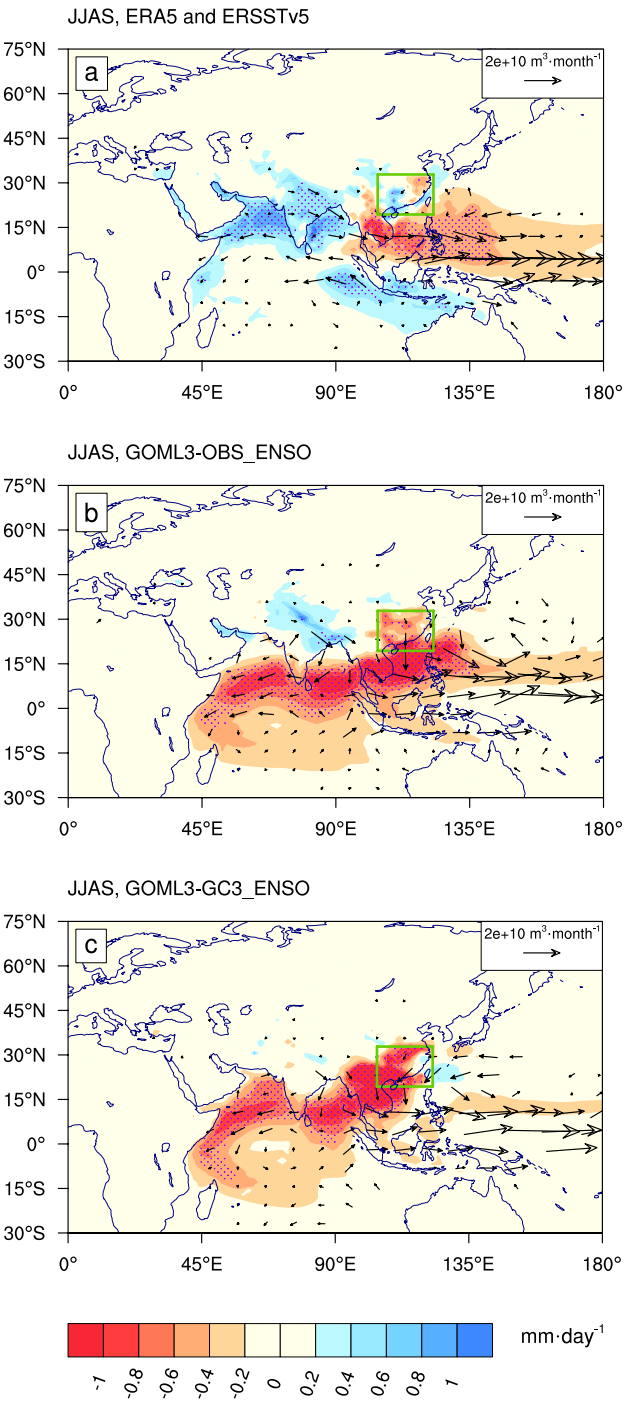

Fig. 10 JJAS tracked moisture sources of rainfall (shaded, mmday^{-1}) and tracked vertically integrated moisture transport (arrows, m^3 month^{-1}) for the South China box (green box) obtained using the WAM-2layers, regressed onto standardised JJAS Niño 3.4 SSTs for **a** ERA5, **b** GOML3-OBS_ENSO, and **c** GOML3-GC3_ENSO. Stippling indicates moisture sources significant at the 5% level using the Student's t-test. Vertically integrated moisture transport vectors are drawn in black color when at least one of the components of the vector is significant at the 5% level using the Student's t-test

3.4.2 IOD

To analyse errors in the IOD teleconnection pathways to the EASM, we linearly regress GOML3-OBS_IOD and GOML3-GC3_IOD simulations of seasonal meteorological variables onto the standardised seasonal IOD index. In this study, the IOD index is calculated as the difference between SST anomalies of two regions of the tropical Indian Ocean, named IOD west (50° E–70° E longitude, 10° S–10°

N latitude) and IOD east (90° E–110° E longitude, 10° S–0° S latitude) (Saji et al. 1999). Similarly, we calculate observed linear regressions of seasonal SSTs of ERSSTv5 and ERA5 meteorological variables onto standardised seasonal IOD index calculated with ERSSTv5 data.

JJAS ERSSTv5 SSTs regressed onto the observed IOD index show a typical pattern of the positive IOD (Fig. 11a). In addition, ERA5 anomalous southeasterlies at 850 hPa, which extend from the Tasman Sea to the equatorial Indian Ocean (to ≈ 60° E), are positively correlated with the IOD index [as in Saji et al. (1999)]. Simultaneously, this regression analysis also shows significant anomalous low-level, westerly winds over continental India and the Bay of Bengal, extending east to reach the equatorial Pacific Ocean.

GOML3-OBS_IOD SSTs and 850 hPa wind regression analysis show southeasterlies over the equatorial Indian Ocean and the Bay of Bengal that are positively correlated with the IOD index (Fig. 11b). This significant circulation continues towards the Bay of Bengal, where anomalous westerlies extend from the Indochinese peninsula to the Pacific Ocean (at ≈ 15° N latitude).

Differences between ERSSTv5 and GOML3-OBS_IOD-regressed SSTs are found in the Tasman Sea, the east side of the Maritime Continent, and the subtropical North Pacific. GOML3-OBS_IOD circulation biases are found in the Pacific Ocean, where anomalous 850 hPa easterlies in positive IOD years are further north than in ERA5. This change in the circulation influences the southward flank of an anomalous weakened WNPSH centred over the Philippine Sea. The GOML3-GC3_IOD 850 hPa easterlies over the South China Sea and the Indochinese peninsula oppose the direction of ERA5-regressed winds.

JJAS ERA5 rainfall in southeast China is positively correlated with the IOD index with regressions up to 0.5 mm day^{-1} and negatively correlated with south Indian and Australian rainfall (Fig. 12a). Regressed ERA5 rainfall presents a dipole of negative anomalies in the IOD east region with up to 1.5 mm day^{-1} and positive anomalies in the IOD west part of up to 2 mm day^{-1}.

GOML3-OBS_IOD underestimates the magnitude of anomalous rainfall in both IOD west and IOD east regions, with about 1 mm day^{-1} biases in both cases. For positive IOD, GOML3-OBS_IOD shows less rainfall than ERA5 over most South East China, the East China Sea, and Bangladesh and more precipitation in Australia (Fig. 12b).

On the other hand, GOML3-GC3_IOD shows more rainfall in positive IOD than GOML3-OBS_IOD in southeastern China, Bangladesh, Myanmar, and Australia (Fig. 12c). This analysis suggests that GOML3-GC3_IOD presents positive changes in the regression slope against GOML3-OBS_IOD during positive IOD events. As a result, GOML3-GC3_IOD offers a better estimation of the sign of anomalous rainfall over southeastern China. Different from the negative rainfall biases in GOML3-GC3gbl (Fig. 6d) during JJAS, GOML3-GC3_IOD regressed slope shows a positive difference in rainfall over southeastern China. This analysis suggests that during IOD episodes, GOML3_GC3 represents the correct sign of rainfall anomalies over EASM rainfall over most of southeast China.

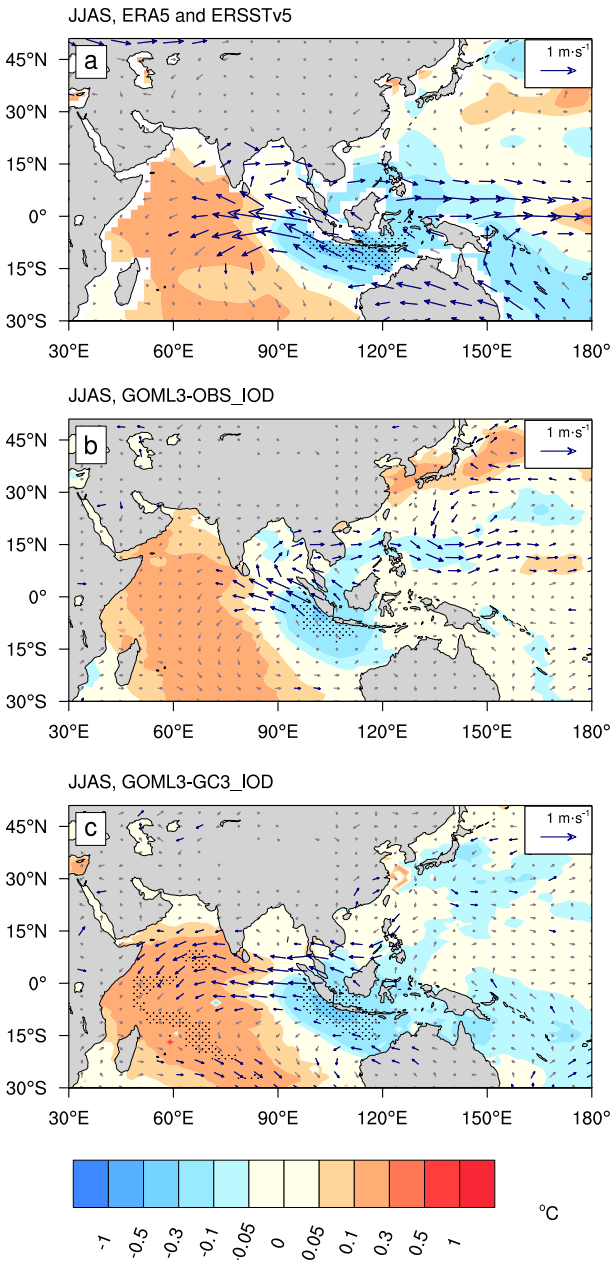

Fig. 11 Mean JJAS SSTs (shaded, °C) and winds at 850 hPa (arrows, ms^{-1}) regressed onto standardised JJAS IOD index for **a** ERA5 and ERSSTv5, **b** GOML3-OBS_IOD, and **c** GOML3-GC3_IOD. Stippling indicates SSTs significant at the 5% level using the Student's t-test. Wind vectors are drawn in navy blue color when at least one of the components of the vector is significant at the 5% level using the Student's t-test

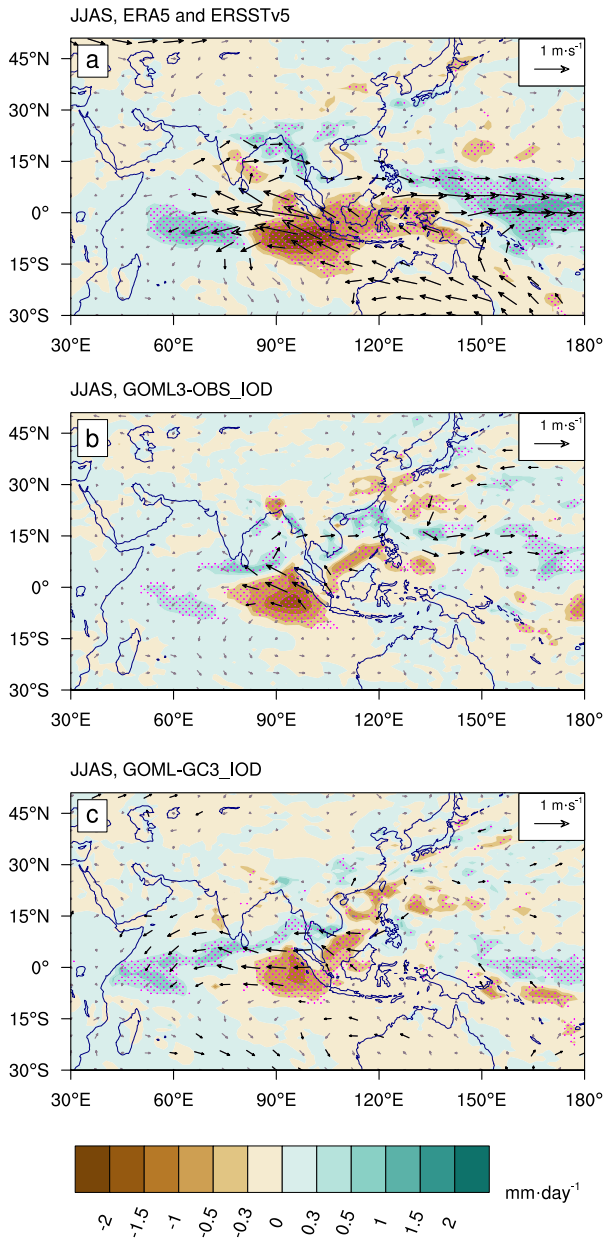

Fig. 12 Mean JJAS precipitation (shaded, mm day^{-1}) and winds at 850 hPa (arrows, ms^{-1}) regressed onto standardised JJAS IOD index for **a** ERA5 and ERSSTv5, **b** GOML3-OBS_IOD, and **c** GOML3-GC3_IOD. Stippling indicates indicates precipitation significant at the 5% level using the Student's t-test. Wind vectors are drawn in navy color when at least one of the components of the vector is significant at the 5% level using the Student's t-test

To investigate the errors in the IOD teleconnection pathways to the EASM, we compute the moisture sources for JJAS rainfall for the South China box. First, we determine the moisture sources for precipitation over this box in ERA5 and GOML3 experiments using the WAM-2layers back trajectory tool (Fig. 13).

ERA5 regressed moisture sources show that in IOD positive years, increased evaporation from the IOD west region, the Bay of Bengal, and the Arabian Sea, precipitates over the south China box (Fig. 13a). Increased moisture transport from these regions is related to increased rainfall over the South China box.

Regression analysis shows that GOML3-OBS_IOD underestimates moisture sources over continental China and the east IOD region, which contributes to less rainfall in the south China box with GOML3-OBS_IOD (Fig. 13b). GOML3-OBS_IOD experiments also have a strong positive moisture bias that extends from Laos to the Philippines, larger than 1 mm month^{-1}. Regressed moisture transports from the Philippine Sea are weaker than that in ERA5.

GOML3-OBS_IOD underestimate moisture sources from the South China Sea, IOD east, the Bay of Bengal, the Arabic Sea, and India (Fig. 13c). However, GC3 SST biases enhance the EASM flow. Therefore, GC3 corrects the underestimation of moisture sources in east IOD and southeast China from GOML3-OBS_IOD, and the moisture transport in the Indian Ocean is better represented with GC3.

4 Discussion and summary

In this study, we analyse simulations from the MetUM-GOML3, coupled model of the MetUM GA7 atmosphere to a mixed-layer ocean, which constrains the SSTs to observations (GOML3-OBS) or GC3 SSTs. Furthermore, the GOML3-OBS experiment is used as a reference to analyse different coupled climate-length MetUM-GC3 runs.

GOML experiments with global GC3 SST biases allow us to establish the effects of regional SST errors on the EASM, in which GC3 global SST biases cause a substantial shift in the seasonal cycle of the EASM: a late northward progression of the monsoon in June, and an early retreat of the EASM (early August) reduces rainfall over most of northern China.

Another set of GOML experiments with individual regional SST biases in the Atlantic, Pacific, and Indian Oceans allow us to establish the effects of basin-scale SST errors on the EASM. This approach helps test the remote influence of the three different ocean basins on the EASM.

It is found that the simulated rainfall over East Asia is more sensitive to SST errors in the Indian and Pacific oceans than those in the Atlantic Ocean. However, these analyses show the cancellation of effects between Pacific Ocean biases and Atlantic and Indian Ocean biases. GC3 SST biases in the Indian and Atlantic Oceans reduce JJAS rainfall over most southeastern China. In both cases, these conditions are related to a later northward EASM progression and an earlier monsoon retreat during September. Conversely, GC3 Pacific SST biases increase rainfall over

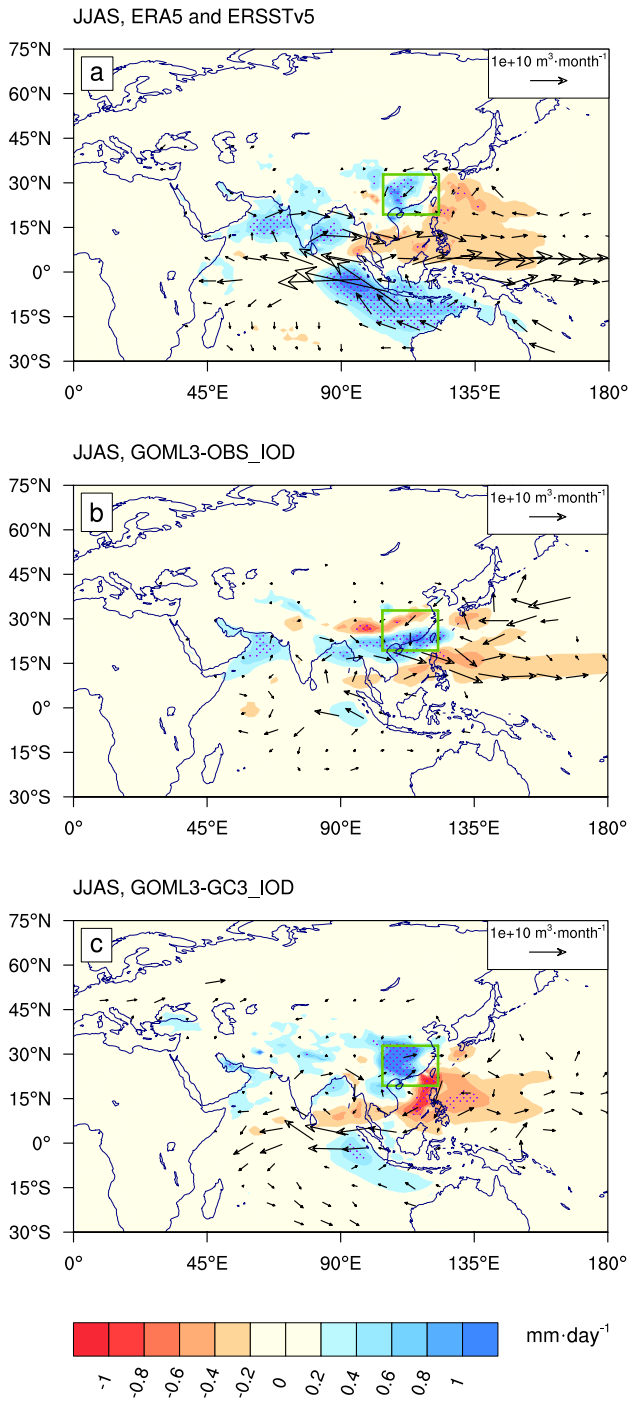

Fig. 13 JJAS tracked moisture sources of rainfall (shaded, mmday^{-1}) and tracked vertically integrated moisture transport (arrows, m^3 month^{-1}) for the South China box (green box) obtained using the WAM-2layers, regressed onto standardised JJAS IOD index for **a** ERA5, **b** GOML3-OBS_IOD, and **c** GOML3-GC3_IOD. Stippling indicates moisture sources significant at the 5% level. Vertically integrated moisture transport vectors are drawn in black color when at least one of the components of the vector is significant at the 5% level

southeastern China, associated with a systematic increase of moisture convergence in the equatorial West Pacific and southeast China and moisture divergence in the Philippine and South China Sea.

An essential finding of the GOML experiments is the opposite effect of the Pacific and the Atlantic Ocean SST biases on the North Pacific circulation. An increase (decrease) in EASM rainfall is linked to an enhanced (weakened) North Pacific subtropical high circulation. In both cases, changes in the circulation in the West Pacific, near the Philippines, play a key role in the biases of local evaporation and moisture transport towards South China.

Our study shows that MetUM-GOML3 presents similar cold SST biases in the Indian Ocean as its predecessors (Levine and Turner 2012; Levine et al. 2021). The low-level winds and rainfall associated with these SST biases characterise an enhanced Indian summer Monsoon. Additionally, our WAM-2layers analysis shows that evaporation and moisture transport biases in the Indian Ocean result in more extensive EASM changes in rainfall. This coincides with multiple studies that found that the Indian Ocean provides the largest amount of moisture during boreal summer for rainfall in southeastern EA (Guo et al. 2019; Sun et al. 2015; Baker et al. 2015).

This study also determined how GC3 SST biases affect the ENSO and the IOD teleconnection to the EASM. The results indicate that ENSO-associated rainfall anomalies over South China are not correctly simulated with the GOML model, even with observed climatological SSTs (Fig. 9).

GOML3 experiments do not accurately represent the equatorward anomalous rainfall migration during the warm episodes of ENSO, which is associated with an anomalous equatorward migration of the ITCZ. In addition, among the GOML3 biases during ENSO, we found anomalous lower troposphere westerly winds located further northwards along the tropical Pacific. Therefore, MetUM-GOML3 experiments have an incorrect sign of the anomalous moisture sources related to the anomalous seasonal rainfall over South China, simulating reduced moisture sources of rainfall in the Bay of Bengal and the Arabian Sea. GC3 SSTs biases worsen the bias of ENSO-associated precipitation over South China, being related to amplified biases of an anomalous moisture source, mainly in the Philippine Sea, the Indian Ocean, and the Tibetan Plateau.

Finally, the effect of GC3 SST biases on the simulated IOD teleconnection to the EASM is studied. The circulation biases are widely found in the tropical Pacific Ocean, where anomalous low-level winds are located further north. This is associated with biases in the intensity and location of the WNPSH and its variability, which strongly influences the location and strength of the GOML3 representation of the EASM rainfall.

Acknowledgements The authors thank the two anonymous reviewers for their constructive comments to improve the manuscript. This work and its contributors (Armenia Franco-Díaz, Nicholas P. Klingaman, Andrew G. Turner, Liang Guo, and Buwen Dong) were supported by the UK-China Research & Innovation Partnership Fund through the Met Office Climate Science for Service Partnership (CSSP) China as part of the Newton Fund. The MetUM-GOML simulations were supported by the UK National Supercomputing Service ARCHER.

Author contributions NPK performed the model integrations. AFD performed the analysis in consultation with AGT, NPK, LG, and BD. AFD prepared the paper with contributions from NPK, AGT, and BD.

Funding This research has been supported by the Newton Fund (CSSP China).

Data availability The MetUM was used under licence from the UK Met Office; for details, see https://www.metoffice.gov.uk/research/modelling-systems/unified-model. Data and code will be available upon request through JASMIN (http://www.jasmin.ac.uk/). MetUM simulation data are available via the National Centre for Atmospheric Science and the UK Met Office; access is restricted.

Declarations

Conflict of interest The authors declare no conflict of interest.

Consent for publication Not applicable.

Consent to participate Not applicable.

Ethics approval Not applicable.

References

Adler RF, Sapiano MRP, Huffman GJ, Wang J-J, Gu G, Bolvin D, Chiu L, Schneider U, Becker A, Nelkin E, Xie P, Ferraro R, Shin D-B (2018) The global precipitation climatology project (GPCP) monthly analysis (new version 2.3) and a review of 2017 global precipitation. Atmosphere 9(4):138. https://doi.org/10.3390/atmos9040138

Alexander M, Scott J (2002) The influence of ENSO on air–sea interaction in the Atlantic. Geophys Res Lett 29(14):46–1464. https://doi.org/10.1029/2001GL014347

Baker AJ, Sodemann H, Baldini JUL, Breitenbach SFM, Johnson KR, van Hunen J, Zhang P (2015) Seasonality of westerly moisture transport in the East Asian summer monsoon and its implications for interpreting precipitation. J Geophys Res Atmos 120(12):5850–5862. https://doi.org/10.1002/2014JD022919

Berry G, Reeder MJ (2014) Objective identification of the intertropical convergence zone: climatology and trends from the ERA-interim. J Clim 27(5):1894–1909. https://doi.org/10.1175/JCLI-D-13-00339.1

Cai W, Cowan T (2013) Why is the amplitude of the Indian Ocean dipole overly large in CMIP3 and CMIP5 climate models? Geophys Res Lett 40(6):1200–1205. https://doi.org/10.1002/grl.50208

Dai A, Li H, Sun Y, Hong L-C, LinHo, Chou C, Zhou T (2013) The relative roles of upper and lower tropospheric thermal contrasts and tropical influences in driving Asian summer monsoons. J Geophys Res Atmos 118(13):7024–7045. https://doi.org/10.1002/jgrd.50565

Dee DP, Uppala SM, Simmons AJ, Berrisford P, Poli P, Kobayashi S, Andrae U, Balmaseda MA, Balsamo G, Bauer P, Bechtold P, Beljaars ACM, van de Berg L, Bidlot J, Bormann N, Delsol C, Dragani R, Fuentes M, Geer AJ, Haimberger L, Healy SB, Hersbach H, Hólm EV, Isaksen L, Kållberg P, Köhler M, Matricardi M, McNally AP, Monge-Sanz BM, Morcrette J-J, Park B-K, Peubey C, de Rosnay P, Tavolato C, Thépaut J-N, Vitart F (2011) The ERA-interim reanalysis: configuration and performance of the data assimilation system. Q J R Meteorol Soc 137(656):553–597. https://doi.org/10.1002/qj.828

Ding H, Greatbatch RJ, Park W, Latif M, Semenov VA, Sun X (2014) The variability of the East Asian summer monsoon and its relationship to ENSO in a partially coupled climate model. Clim Dyn 42(1):367–379. https://doi.org/10.1007/s00382-012-1642-3

Fu Y, Lu R (2017) Improvements in simulating the relationship between ENSO and East Asian summer rainfall in the CMIP5 models. J Clim 30(12):4513–4525. https://doi.org/10.1175/JCLI-D-16-0606.1

Fu Y, Lu R, Wang H, Yang X (2013) Impact of overestimated ENSO variability in the relationship between ENSO and East Asian summer rainfall. J Geophys Res Atmos 118:6200–6211. https://doi.org/10.1002/jgrd.50482

Gill AE (1980) Some simple solutions for heat-induced tropical circulation. Quar J R Meteorol Soc 106:447–462. https://doi.org/10.1002/qj.49710644905

Guo L, van der Ent RJ, Klingaman NP, Demory M-E, Vidale PL, Turner AG, Stephan CC, Chevuturi A (2019) Moisture sources for east asian precipitation: mean seasonal cycle and interannual variability. J Hydrometeorol 20(4):657–672. https://doi.org/10.1175/JHM-D-18-0188.1

Guo L, van der Ent RJ, Klingaman NP, Demory M-E, Vidale PL, Turner AG, Stephan CC, Chevuturi A (2020) Effects of horizontal resolution and air-sea coupling on simulated moisture source for East Asian precipitation in MetUM GA6/GC2. Geosci Model Dev 13(12):6011–6028. https://doi.org/10.5194/gmd-13-6011-2020

Ha K-J, Chu J-E, Lee J-Y, Yun K-S (2017) Interbasin coupling between the tropical Indian and Pacific Ocean on interannual timescale: observation and CMIP5 reproduction. Clim Dyn 48(1):459–475. https://doi.org/10.1007/s00382-016-3087-6

He C, Zhou T (2014) The two interannual variability modes of the Western North Pacific Subtropical High simulated by 28 CMIP5-AMIP models. Clim Dyn 43:2455–2469. https://doi.org/10.1007/s00382-014-2068-x

Hersbach H, Bell B, Berrisford P, Hirahara S, Horányi A, Muñoz-Sabater J, Nicolas J, Peubey C, Radu R, Schepers D et al (2020) The ERA5 global reanalysis. Q J R Meteorol Soc 146(730):1999–2049. https://doi.org/10.1002/qj.3803

Hirons LC, Klingaman NP, Woolnough SJ (2015) MetUM-GOML: a near-globally coupled atmosphere-ocean-mixed-layer model. Geosci Model Dev 8:363–379. https://doi.org/10.5194/gmd-8-363-2015

Huang B, Thorne PW, Banzon VF, Boyer T, Chepurin G, Lawrimore JH, Menne MJ, Smith TM, Vose RS, Zhang H-M (2017) Extended reconstructed sea surface temperature, version 5 (ERSSTv5):

upgrades, validations, and intercomparisons. J Clim 30(20):8179–8205. https://doi.org/10.1175/JCLI-D-16-0836.1
Jiang D, Tian Z, Lang X (2016) Reliability of climate models for China through the IPCC Third to Fifth Assessment Reports. Int J Climatol 36(3):1114–1133. https://doi.org/10.1002/joc.4406
Jiang W, Li G, Wang G (2021) Effect of the El Niño decaying pace on the East Asian summer monsoon circulation pattern during post-El Niño summers. Atmosphere 12(2):140. https://doi.org/10.3390/atmos12020140
Jiao D, Xu N, Yang F, Xu K (2021) Evaluation of spatial-temporal variation performance of ERA5 precipitation data in China. Sci Rep 11(1):17956. https://doi.org/10.1038/s41598-021-97432-y
Klingaman NP, Demott CA (2020) Mean state biases and interannual variability affect perceived sensitivities of the Madden–. J Adv Model Earth Syst 12(2):e2019MS001799. https://doi.org/10.1029/2019MS001799
Kusonoki S, Yoshimura J, Yoshimura H, Noda A, Oouchi K, Mizuta R (2006) Change of Baiu Rain Band in global warming projection by an atmospheric general circulation model with a 20-km grid size. J Meteorol Soc Jpn Ser II 84(4):581–611. https://doi.org/10.2151/jmsj.84.581
Lau N-C, Ploshay JJ (2009) Simulation of synoptic- and subsynoptic-scale phenomena associated with the East Asian summer monsoon using a high-resolution GCM. Mon Weather Rev 137(1):137–160. https://doi.org/10.1175/2008MWR2511.1
Lee S-S, Seo Y-W, Ha K-J, Jhun J-G (2013) Impact of the western North Pacific subtropical high on the East Asian monsoon precipitation and the Indian Ocean precipitation in the boreal summertime. Asia-Pac J Atmos Sci 49(2):171–182. https://doi.org/10.1007/s13143-013-0018-x
Levine RC, Turner AG (2012) Dependence of indian monsoon rainfall on moisture fluxes across the Arabian Sea and the impact of coupled model sea surface temperature biases. Clim Dyn 38(11):2167–2190. https://doi.org/10.1007/s00382-011-1096-z
Levine RC, Klingaman NP, Peatman SC, Martin GM (2021) Roles of air-sea coupling and horizontal resolution in the climate model simulation of Indian monsoon low pressure systems. Clim Dyn 56:1203–1226. https://doi.org/10.1007/s00382-020-05526-6
Li X, Zhou W (2012) Quasi-4-yr coupling between El Niño-Southern Oscillation and water vapor transport over East Asia-WNP. J Clim 25:5879–5891. https://doi.org/10.1175/JCLI-D-11-00433.1
Li S, Lu J, Huang G, Hu K (2008) Tropical Indian Ocean basin warming and East Asian summer monsoon: a multiple AGCM study. J Clim 21:6080–6088. https://doi.org/10.1175/2008JCLI2433.1
Li C, Scaife AA, Lu R, Arribas A, Brookshaw A, Comer RE, Li J, MacLachlan C, Wu P (2016) Skillful seasonal prediction of Yangtze river valley summer rainfall. Environ Res Lett 11:094002. https://doi.org/10.1088/1748-9326/11/9/094002
Li Y, Deng Y, Yang S, Zhang H, Ming Y, Shen Z (2019) Multi-scale temporal-spatial variability of the East Asian summer monsoon frontal system: observation versus its representation in the GFDL HiRAM. Clim Dyn 52(11):6787–6798. https://doi.org/10.1007/s00382-018-4546-z
Liu J, Wang B, Yang J (2008) Forced and internal modes of variability of the East Asian summer monsoon. Clim Past 4(4):225–233. https://doi.org/10.5194/cp-4-225-2008
Matsuno T (1966) Quasi-geostrophic motions in the equatorial area. J Meteorol Soc Jpn 44:25–43. https://doi.org/10.2151/jmsj1965.44.1_25
Nogueira M (2020) Inter-comparison of ERA-5, ERA-interim and GPCP rainfall over the last 40 years: process-based analysis of systematic and random differences. J Hydrol 583:124632. https://doi.org/10.1016/j.jhydrol.2020.124632
Peatman SC, Klingaman NP (2018) The Indian summer monsoon in MetUM-GOML2.0: effects of air–sea coupling and resolution. Geosci Model Dev 11(11):4693–4709. https://doi.org/10.5194/gmd-11-4693-2018
Rodríguez JM, Milton SF (2019) East Asian summer atmospheric moisture transport and its response to interannual variability of the west Pacific subtropical high: an evaluation of the met office unified model. Atmosphere 10(8):457. https://doi.org/10.3390/atmos10080457
Saji NH, Goswami BN, Vinayachandran PN, Yamagata T (1999) A dipole mode in the tropical Indian Ocean. Nature 401:360–363. https://doi.org/10.1038/43854
Smith DM, Murphy JM (2007) An objective ocean temperature and salinity analysis using covariances from a global climate model. J Geophys Res Oceans. https://doi.org/10.1029/2005JC003172
Song F, Zhou T (2014) Interannual variability of East Asian summer monsoon simulated by CMIP3 and CMIP5 AGCMs: skill dependence on Indian ocean-western pacific anticyclone teleconnection. J Clim 27(4):1679–1697. https://doi.org/10.1175/JCLI-D-13-00248.1
Sperber KR, Annamalai H, Kang I-S, Kitoh A, Moise A, Turner A, Wang B, Zhou T (2013) The Asian summer monsoon: an intercomparison of CMIP5 vs. CMIP3 simulations of the late 20th century. Clim Dyn 42(9):2711–2744. https://doi.org/10.1007/s00382-012-1607-6
Stephan CC, Klingaman NP, Vidale PL, Turner AG, Demory M-E, Guo L (2018) Interannual rainfall variability over China in the MetUM GA6 and GC2 configurations. Geosci Model Dev 11(5):1823–1847. https://doi.org/10.5194/gmd-11-1823-2018
Stephan CC, Klingaman NP, Turner AG (2019) A mechanism for the recently increased interdecadal variability of the Silk Road pattern. J Clim 32(3):717–736. https://doi.org/10.1175/JCLI-D-18-0405.1
Sun B, Wang H (2015) Analysis of the major atmospheric moisture sources affecting three sub-regions of East China. Int J Climatol 35(9):2243–2257. https://doi.org/10.1002/joc.4145
van der Ent RJ, Tuinenburg OA, Knoche H-R, Kunstmann H, Savenije HHG (2013) Should we use a simple or complex model for moisture recycling and atmospheric moisture tracking? Hydrol Earth Syst Sci 01(17):4869–4884. https://doi.org/10.5194/hess-17-4869-2013
van der Ent RJ, Wang-Erlandsson L, Keys PW, Savenije HHG (2014) Contrasting roles of interception and transpiration in the hydrological cycle—Part 2: moisture recycling. Earth Syst Dyn 5(2):471–489. https://doi.org/10.5194/esd-5-471-2014
Walters D, Baran AJ, Boutle I, Brooks M, Earnshaw P, Edwards J, Furtado K, Hill P, Lock A, Manners J et al (2019) The Met Office Unified Model global atmosphere 7.0/7.1 and JULES global land 7.0 configurations. Geosci Model Dev 12(5):1909–1963. https://doi.org/10.5194/gmd-12-1909-2019
Wang B, Wu R, Fu X (2000) Pacific-East Asian teleconnection: how does ENSO affect East Asian climate? J Clim 13(9):1517–1536. https://doi.org/10.1175/1520-0442(2000)013<1517:PEATHD>2.0.CO;2
Wang B, Wu Z, Li J, Liu J, Chang C-P, Ding Y, Wu G (2008) How to measure the strength of the East Asian summer monsoon. J Clim 21(17):4449–4463. https://doi.org/10.1175/2008JCLI2183.1
Wang B, Xiang B, Lee J-Y (2013) Subtropical High predictability establishes a promising way for monsoon and tropical storm predictions. Proc Natl Acad Sci USA 110(8):2718–2722. https://doi.org/10.1073/pnas.1214626110
Wang G, Cai W, Santoso A (2017) Assessing the impact of model biases on the projected increase in frequency of extreme positive Indian Ocean dipole events. J Clim 30(8):2757–2767. https://doi.org/10.1175/JCLI-D-16-0509.1
Weller E, Cai W (2013) Realism of the Indian Ocean dipole in CMIP5 models: the implications for climate projections. J Clim 26(17):6649–6659. https://doi.org/10.1175/JCLI-D-12-00807.1

Williams KD, Copsey D, Blockley EW, Bodas-Salcedo A, Calvert D, Comer R, Davis P, Graham T, Hewitt HT, Hill R, Hyder P, Ineson S, Johns TC, Keen AB, Lee RW, Megann A, Milton SF, Rae JGL, Roberts MJ, Scaife AA, Schiemann R, Storkey D, Thorpe L, Watterson IG, Walters DN, West A, Wood RA, Woolings T, Xavier PK (2017) The met office global coupled model 3.0 and 3.1 (GC3.0 and GC3.1) configurations. J Adv Model Earth Syst 10:357–380. https://doi.org/10.1002/2017MS001115

Wu R, Kirtman BP, Pegion K (2006) Local air-sea relationship in observations and model simulations. J Clim 19(19):4914–4932. https://doi.org/10.1175/JCLI3904.1

Wu C-H, Freychet N, Chen C-A, Hsu H-H (2017) East Asian pre-summer precipitation in the CMIP5 at high versus low horizontal resolution. Int J Climatol 37(11):4158–4170. https://doi.org/10.1002/joc.5055

Xie S-P, Hu KM, Hafner J, Tokinaga H, Du Y, Huang G, Sampe T (2009) Indian Ocean capacitor effect on Indo-western Pacific climate during the summer following El Niño. J Clim 22:730–747. https://doi.org/10.1175/2008JCLI2544.1

Xie S-P, Kosaka Y, Du Y, Hu KM, Chowdary JS, Huang G (2016) Indo-western Pacific Ocean capacitor and coherent climate anomalies in post-ENSO summer: a review. Adv Atmos Sci 33:411–432. https://doi.org/10.1007/s00376-015-5192-6

Yuan Y, Yang H, Zhou W, Li C (2008) Influences of the Indian Ocean dipole on the Asian summer monsoon in the following year. Int J Climatol 28(14):1849–1859. https://doi.org/10.1002/joc.1678